



# 1 **Changes in satellite retrievals of atmospheric composition over** 2 **eastern China during the 2020 COVID-19 lockdowns**

3  
4 Robert D. Field<sup>1,2</sup>, Jonathan E. Hickman<sup>1</sup>, Igor V. Geogdzhayev<sup>1,2</sup>, Kostas Tsigaridis<sup>1,3</sup>, Susanne E. Bauer<sup>1</sup>

5  
6 <sup>1</sup>NASA Goddard Institute for Space Studies, 2880 Broadway, New York, NY, USA, 10025

7 <sup>2</sup>Dept. of Applied Physics and Applied Mathematics, Columbia University 2880 Broadway, New York, NY,  
8 USA, 10025

9 <sup>3</sup>Center for Climate Systems Research, Columbia University, 2880 Broadway, New York, NY, USA, 10025

10 *Correspondence to:* Robert D. Field (robert.field@columbia.edu)

11 **Abstract.** We examined daily Level-3 satellite retrievals of AIRS CO, OMI SO<sub>2</sub> and NO<sub>2</sub>, and MODIS AOD  
12 over eastern China to understand how COVID-19 lockdowns affected atmospheric composition, taking into  
13 account trends that have occurred since 2005. Over central east China during the January 23 - April 8 lockdown  
14 window, CO in 2020 was 12% lower than the 2005-2019 mean, but only 2% lower than what would be expected  
15 given the decreasing CO trend over that period. Similarly for AOD, 2020 was 30% lower than the 2011-2019  
16 mean, but not distinct from what would be expected from the trend. NO<sub>2</sub> in 2020 was 43% lower than the 2011-  
17 2019 mean, but only 17% lower than what would be expected given the trend over that period. Over southern  
18 China, 2020 NO<sub>2</sub> was not significantly different from anticipated, and CO and AOD were significantly higher than  
19 what would be expected, which we suggest was partly because of an active fire season in neighbouring countries.  
20 Over east central and southern China, SO<sub>2</sub> was higher than expected, but the magnitude depended strongly on  
21 how daily regional values were calculated from individual retrievals. Future work over China, or other regions,  
22 needs to take these trends into account in order to separate the effects of COVID-19 on air quality from recent  
23 trends, or from variability in other sources.

## 24 **1 Introduction**

25 In an effort to control the spread of COVID-19, the Chinese government implemented a range of restrictions on  
26 movement. These led to reductions in industrial and other work related and personal activities starting January  
27 23, 2020 in Wuhan, Hubei province, then extending to other cities and regions in the days that followed. On April  
28 8, 2020, Wuhan was the last city to re-open after a complete lockdown that prevented most people from leaving  
29 their homes. These measures have been linked to changes in air quality. A network of surface monitoring stations  
30 in northern China observed 35% decreases in PM<sub>2.5</sub> and 60% decreases in NO<sub>2</sub> concentrations during January 29  
31 through February 29, as compared to the preceding three weeks; CO and SO<sub>2</sub> also declined (Shi and Brasseur,  
32 2020). In and around Wuhan, decreases of NO<sub>2</sub> and PM<sub>2.5</sub> were similar to regional changes, but there was a slight  
33 increase in SO<sub>2</sub> concentrations (Shi and Brasseur, 2020). Observations by the Tropospheric Monitoring Instrument  
34 (TROPOMI) showed large decreases in tropospheric NO<sub>2</sub> column densities over Chinese cities, on the order of  
35 40% for February 11 to March 24 2020 compared to the same period in 2019, ranging from roughly 25% for cities  
36 not affected by lockdown to 60% for Wuhan and Xi'an (Bauwens et al., 2020). Prospective simulations suggested  
37 that meteorology may limit the effect of reduced emissions on PM<sub>2.5</sub> concentrations, with Chinese cities  
38 experiencing less than 20% reductions (Wang et al., 2020).



39

40 The goal of our study was to consider these changes against pollution trends in China using NASA Earth  
41 Observing System data by combining several products to give a holistic view covering several emission sectors  
42 that are responsible for the observed changes. Over the last 2 to 3 decades, air pollution in China appears to have  
43 followed the pattern described by the Environmental Kuznets Curve (Selden and Song, 1994). This framework  
44 describes a relationship in which economic growth is initially accompanied by an increase in air pollution, when  
45 poverty remains widespread. But as growth continues, air pollution is expected to level off and decline as a  
46 consequence of changes in social awareness of environmental degradation and the economic, political, and  
47 technological capacity to limit it (Sarkodie and Strezov, 2019; Selden and Song, 1994).

48

49 Bottom-up and top-down assessments of air pollutant emissions and concentrations suggest that China has  
50 followed this pattern during the era of satellite monitoring of atmospheric composition, with concentrations of  
51 SO<sub>2</sub>, NO<sub>2</sub>, CO, and aerosol optical depth (AOD) mostly exhibiting marked and steady declines over the last  
52 decade. In the case of NO<sub>2</sub>, multi-instrument analyses, which extend the observational record beyond the lifetime  
53 of a single instrument, depict a consistent regional picture of NO<sub>2</sub> trends in China since 1996 (Geddes et al.,  
54 2016; Georgoulias et al., 2019; Wang and Wang, 2020; Xu et al., 2020). Column totals show an increasing trend  
55 during the first part of the satellite record, but this trend is reversed sometime between 2010 and 2014 (Georgoulias  
56 et al., 2019; Krotkov et al., 2016; Lin et al., 2019; Xu et al., 2020; Si et al., 2019; Shah et al., 2020). The trend reversal  
57 has been attributed to a combination of emission control measures (Zheng et al., 2018a) and variations in economic  
58 growth (Krotkov et al., 2016).

59

60 Bottom-up estimates suggest that SO<sub>2</sub> emissions peaked earlier, with declines starting around 2005, primarily as  
61 a result of power and industrial pollution control measures as well as the elimination of small industrial boilers  
62 (Sun et al., 2018; Zheng et al., 2018b). An earlier peak in SO<sub>2</sub> emissions is consistent with observations by multiple  
63 satellite instruments, which revealed declines in SO<sub>2</sub> column densities since 2005 (Fioletov et al., 2016; Krotkov  
64 et al., 2016; Wang and Wang, 2020; Zhang et al., 2017; Si et al., 2019).

65

66 AOD retrievals from the Along Track Scanning Radiometer instruments show a steady increase over southeastern  
67 China from 1995 to 2005 (Sogacheva et al., 2020), and declines thereafter in the MODIS AOD (He et al., 2019).  
68 The AOD peak has been argued to match either the ~2011 peak in NO<sub>2</sub> (Zheng et al., 2018b; Xie et al., 2019), the  
69 ~2005 peak of SO<sub>2</sub>, with more rapid decreases in AOD after 2011 (Lin et al., 2018), or to have occurred in between  
70 (Ma et al., 2016). The recent decrease in AOD is also seen in VIIRS retrievals (Sogacheva et al., 2020). Most  
71 mitigation of direct PM<sub>2.5</sub> emissions since 2010 was by industry, with residential emissions also decreasing  
72 substantially (Zheng et al., 2018b). The decline in SO<sub>2</sub> emissions also exerted an important influence, with the  
73 sulfate concentration of PM<sub>2.5</sub> decreased substantially between 2013 and 2017 (Shao et al., 2018), reflecting the  
74 negative trend in SO<sub>2</sub> emissions.

75

76 The peak in concentrations of CO, which has an atmospheric lifetime ranging from weeks to months, is less easily  
77 identified. Some studies suggest that trends have been negative potentially throughout the 21<sup>st</sup> century (Han et al.,  
78 2018; Strode et al., 2016; Wang et al., 2018; Yumimoto et al., 2014; Zheng et al., 2018a), but others suggest that



79 emissions and/or column densities were increasing or flat during at least the first decade of the century (Sun et  
80 al., 2018;Zhao et al., 2013;Zhao et al., 2012). The negative trend has been attributed largely to reductions in  
81 emissions from industrial activity, as well as from residential and transportation sectors (Zheng et al.,  
82 2018a;Zheng et al., 2018b).

83  
84 In addition to these long-term trends, a number of air pollutants also exhibit strong seasonal variation in China.  
85 Anthropogenic emissions of CO, SO<sub>2</sub>, and PM<sub>2.5</sub> are highest in winter, reflecting large variation in emissions from  
86 the residential sector and, in the case of CO, increased emissions associated with cold-start processes in the  
87 transportation sector (Li et al., 2017). Outflow of CO and AOD has a spring maximum, resulting from transport  
88 of pollution, dust, and boreal biomass burning emissions (Han et al., 2018;Luan and Jaegle, 2013).

89  
90 Changes in pollution over China have also come from short-term interventions. To improve air quality for the  
91 2008 summer Olympics—a time when emissions in China were high and still increasing—the Chinese  
92 government imposed a series of strict emissions control measures from July through September 21, 2008, which  
93 were qualitatively similar to the emissions reductions expected to have accompanied the COVID-19 lockdown  
94 (UNEP, 2009). As a result, NO<sub>2</sub> concentrations over Beijing were estimated to have declined by between 40%  
95 and 60% based on satellite observations, with substantial but smaller reductions in surrounding cities often on the  
96 order of 20% to 30% compared to previous years (Mijling et al., 2009;Witte et al., 2009). Regional reductions of  
97 SO<sub>2</sub> and CO during the months of the games were estimated to be 13% and 19%, respectively (Witte et al., 2009).  
98 These results are broadly consistent with on-road observations (Wang et al., 2009), but larger than some surface  
99 observations comparing concentrations before and after the emission control measures were implemented (Wang  
100 et al., 2010).

101  
102 The COVID-related lockdowns provide a similar natural experiment to the 2008 Beijing Olympics but on the  
103 other side of the Kuznets curve. The fact that the lockdowns occurred during years of decreasing air pollution  
104 needs to be taken into account in attributing changes in atmospheric composition to COVID-19 lockdowns,  
105 independent of the long-term trend. Following Chen et al.'s (2020) analysis of air quality improvements on  
106 mortality which controlled for changes in air quality since 2016, in this study we determine whether changes in  
107 2020 in satellite retrievals of CO, SO<sub>2</sub>, NO<sub>2</sub> and AOD departed significantly from the expected declines associated  
108 with the long-term decreases in concentrations resulting from pollution controls and technological change.

## 109 **2 Data and methods**

110 We used daily Level-3 (L3) retrievals from four different instruments on three different NASA Earth Observing  
111 System satellites. The Atmospheric Infrared Sounder (AIRS) instrument aboard NASA's Aqua satellite is a 2300-  
112 channel infrared grating spectrometer in a sun-synchronous orbit with northward equator crossing time of 1:30  
113 PM. AIRS carbon monoxide (CO) profiles are retrieved with horizontal resolution of 45 km at nadir, in a swath  
114 of width 30 fields-of-view or about 1600 km. The retrieval uses a cloud-clearing methodology providing CO with  
115 sensitivity that peaks around 500 hPa, with ~0.8-1.2 degrees-of-freedom-of-signal for 50-70% of scenes. More  
116 sampling and higher information content is obtained in clear scenes (Warner et al., 2013). We used the daily  
117 version 6 (AIRS3STD.006) product.



118

119 The Ozone Monitoring Instrument (OMI) aboard NASA's Aura satellite was launched in July 2004, and has a  
120 local equator-crossing time of roughly 13:45. OMI is a nadir-viewing spectrometer, which measures solar  
121 backscatter in the UV-visible range (Krotkov, 2013). We used NASA's L3 tropospheric NO<sub>2</sub> column density  
122 Standard Product v3 (OMNO2d\_003), and the OMI Principle Components Analysis Planetary Boundary Layer  
123 (PBL) SO<sub>2</sub> product (OMSO2e\_003), which grid retrievals to 0.25° resolution (Krotkov et al., 2017; Li et al., 2013).  
124 Both products are cloud-screened; only pixels that are at least 70% cloud-free are included in the NO<sub>2</sub> product,  
125 and those that are at least 80% cloud-free are included in the SO<sub>2</sub> product. The NO<sub>2</sub> product relies on air mass  
126 factors (AMFs) calculated with the assistance of an atmospheric chemical transport model and are sensitive to  
127 model representations of emission, chemistry, and transport data. Instead of AMFs, the SO<sub>2</sub> product uses  
128 spectrally-dependent SO<sub>2</sub> Jacobians, but can be interpreted as having a fixed AMF that is representative of  
129 summertime conditions. We applied basic transient SO<sub>2</sub> plume filtering, excluding retrievals with SO<sub>2</sub> > 15 DU  
130 (Wang and Wang, 2020).

131

132 Because our trend analysis uses a seasonal mean as the response variable, we assume that random errors cancel  
133 out, leaving only systematic errors, which do not contribute to uncertainty in the trend analysis. Systematic errors  
134 in the OMI NO<sub>2</sub> product (associated with AMFs and tropospheric vertical column contents) have an uncertainty  
135 of 20% (McLinden et al., 2014). The OMI NO<sub>2</sub> products use an implicit aerosol correction to account for the  
136 optical effects of aerosols, but retrievals can be biased when aerosol loading is extreme (Castellanos et al., 2015).  
137 Under these conditions, the OMI NO<sub>2</sub> retrieval is biased low by roughly 20 to 40% (Chimot et al., 2016). Note  
138 that any aerosol-related error would have the potential effect of underestimating the magnitude of decreases in  
139 NO<sub>2</sub> column densities when comparing 2020 to previous years. Additional bias in the NO<sub>2</sub> product may be  
140 introduced due to the reliance on nearly cloud-free pixels, in which greater sunlight may induce higher  
141 photochemical rates. For example, the current NO<sub>2</sub> product is biased roughly 30% low over the Canadian oil sands  
142 (McLinden et al., 2014). The level-2 OMI- NO<sub>2</sub> product has been validated against in situ and surface-based  
143 observations showing good agreement (Lamsal et al., 2014). The use of fixed Jacobians in the SO<sub>2</sub> product  
144 introduces systematic errors of 50 to 100% for cloud-free observations (Krotkov et al., 2016).

145

146 Starting in 2007, the quality of level 1B radiance data for some OMI viewing directions has been affected, known  
147 as the row anomaly. The L3 products used here exclude all pixels affected by the row anomaly from each  
148 observation, but the locations of the row anomaly pixels were dynamic between 2007 and 2011, which could  
149 affect any comparisons including those years. Since 2011, the pixels affected by the row anomaly problem are the  
150 same, so comparisons for data only since 2011 are not affected by changes in the row anomaly.

151

152 Moderate Resolution Imaging Spectroradiometer (MODIS) sensors observe the Earth from polar orbit, from Terra  
153 satellite since 2000 and from Aqua since mid 2002. In this study we use MODIS-derived AOD at 550nm obtained  
154 by merging Dark Target and Deep Blue retrievals (Sayer et al., 2014). Specifically, we use the  
155 Deep\_Blue\_Aerosol\_Optical\_Depth\_550\_Land\_Mean field over land and the over ocean  
156 AOD\_550\_Dark\_Target\_Deep\_Blue\_Combined\_Mean the from Collection 6.1 L3 Gridded products MYD08 and  
157 MOD08 (Hubanks et al., 2019), though very few retrievals over ocean are included in our analysis. L3 values are



158 computed on  $1^\circ \times 1^\circ$  spatial grid from L2 AOD products with resolution of  $10 \times 10$  km. Over land 66% of MODIS-  
159 retrieved Dark-target AOD values were shown to be  $\pm 0.05 \pm 0.15 \times$  AOD AERONET-observed values, with high  
160 correlation ( $R = 0.9$ ) (Levy et al., 2010). Around 78% of the Deep Blue retrievals are within the expected error  
161 range of  $\pm 0.05 \pm 0.20 \times$  AOD (Sayer et al., 2013). MODIS AOD data have been extensively used by the modeling  
162 and remote sensing scientific communities and inter-compared with a wide range of satellite AOD products (see  
163 Schutgens et al. (2020) and references therein).

164

165 We analyzed these retrievals over two large regions (Fig. 1). Central east China was comprised of Shaanxi, Hubei,  
166 Anhui, Jiangsu, Shanxi, Henan, Hebei, Shandong, Beijing, and Tianjin provinces. Southern China was comprised  
167 of Guizhou, Guangxi, Hunan, Jiangxi, Guangdong, Fujian and Zhejiang provinces. Daily mean quantities were  
168 calculated across all valid retrievals falling within the provinces comprising the regions. For the OMI  $\text{NO}_2$   
169 columns, individual retrievals were weighted by the L3 ‘Weight’ field, which is proportional to the fraction of the  
170 grid cell with higher-quality retrievals. We also calculated the daily value from the median of all retrievals, to  
171 understand whether individual high values (mainly  $\text{SO}_2$ ) had any effect on the significance of trends or differences  
172 between 2020 and different background periods. Monthly averages were calculated from the daily regional  
173 averages, with each day weighted in the monthly average by the number of valid retrievals so as to not  
174 overrepresent days with little satellite coverage or significant cloud cover. The monthly data were used to visually  
175 identify COVID-19 related changes against background seasonality and trends since 2005.

176

177 We examined the difference in the distribution of daily data during the 2020 January 23 to April 8 lockdown  
178 period to the same period during previous years since 2005. We compared 2020 to 2019, to background periods  
179 ending in 2019 over which trends were consistent, and to the expected value for 2020 estimated from these trends.  
180 We tested the significance of these differences using bootstrap resampling (Efron and Gong, 1983) with a  
181 resampling size of 2000. Given the uncertainty and uneven nature of trends over different parts of China from  
182 previous studies, we identified the start of existing long-term trends for each species by conducting linear  
183 regressions of the change in the four quantities over time for possible start years of 2005 to 2015. Each trend was  
184 estimated from the start year in this range until 2019. We selected the start year for the most significant trend and  
185 used that trend for comparisons to 2020 data.

186

187 We also considered how the analysis depended on the how the lockdown period was defined. Emissions and  
188 pollution can decrease during the Chinese New Year holidays (Chen et al., 2020), which started as early as January  
189 23 in 2012 and as late as February 19 in 2015, complicating COVID-19 related analyses of atmospheric  
190 composition over China (Bauwens et al., 2020; Chen et al., 2020). The timing and extent of lockdowns also varied  
191 between provinces and we assume that ‘slowdowns’ could have happened before or after stricter, official  
192 lockdowns. For example, ground and air transportation remaining below lockdown levels nationally at least  
193 through April 14, 2020 (International Energy Agency, 2020). Excluding the holiday period from all years is a  
194 straightforward approach to excluding any New Year holiday effects but will exclude simultaneous lockdown  
195 effects during the initial, and presumably most strict, stages of the lockdown. Rather than specifying different  
196 combinations of New Year holiday period and provincial-level lockdown timing, we used January 23–April 8 as  
197 our baseline period (which will include all holiday periods since 2005), but examined the sensitivity of the



198 statistics to the length of the lockdown period, namely a longer lockdown period beginning one week earlier and  
199 one week later, and a shorter lockdown beginning one week later and ending one week earlier. In interpreting the  
200 data, we put more confidence in 2020 differences that were insensitive to these choices.

## 201 **3 Results**

### 202 **3.1 Regional patterns and seasonality**

203 Figure 2 shows the 2020 –2019 differences over China during the January 23-April 8 lockdown period for the  
204 four satellite-retrieved quantities. There were decreases of 5-10 ppbv in AIRS CO over central east China (Fig.  
205 2a) and increases of 20-25 ppbv over southern China in 2020 compared to 2019. The increase in southern China  
206 is adjacent to a stronger positive CO anomaly over the upper Mekong regions of Myanmar, Thailand and Laos.  
207 There were no coherent regional changes in OMI SO<sub>2</sub> (Fig. 2b), but rather smaller localized difference of either  
208 sign. There were decreases in NO<sub>2</sub> (Fig. 2c) across central east China exceeding  $8 \times 10^{15}$  molec cm<sup>-2</sup> coincident  
209 with the weaker decrease in CO. Over southern China, there were comparable differences over Guangdong  
210 province, with smaller differences elsewhere. There was a decrease in MODIS AOD (Fig. 2d) in central-east  
211 China coincident with the decreases in CO and NO<sub>2</sub>, but smaller in magnitude. There was a region of higher AOD  
212 in and northeast of the upper Mekong region coincident with the CO increase, both presumably because of biomass  
213 burning.

214  
215 To put the 2020/2019 difference maps in a longer-term and seasonal context, Figure 3 shows monthly averages  
216 of the four retrieved quantities over central east China since 2005. There are seasonal CO peaks in March-April,  
217 June and September, with the minima usually in November and December (Figure 3a). There has been a decrease  
218 since 2005 in CO. The seasonal decrease from January to February in 2020 is similar to that which has occurred  
219 occasionally before, but the CO during February and March 2020 was the lowest for that time of the year since  
220 2005. By April, CO had returned to levels typical of 2015-2019. The main features of the SO<sub>2</sub> are that it has  
221 decreased since 2005 (Figure 3b), and that early 2020 SO<sub>2</sub> was within the range of recent levels. There is a strong  
222 seasonal NO<sub>2</sub> cycle (Figure 3c), with a July-August minimum, and December-January peak, which has been  
223 attributed to increased heating needs (Yu et al., 2017; Si et al., 2019) and longer chemical lifetime owing to lower  
224 OH and RO<sub>2</sub> (Shah et al., 2020). NO<sub>2</sub> has also decreased since 2011, and during most years, there is a departure  
225 from a smooth seasonal cycle in January and February associated with the Chinese New Year holiday period.  
226 January and February 2020 NO<sub>2</sub> was considerably lower than previous years, increased during March, and had  
227 recovered to typical, recent levels by April. AOD has consistent seasonal peaks in summer which have been  
228 attributed to hygroscopic growth and agricultural residue burning (Filonchik et al., 2019), but had less regular  
229 seasonality otherwise, and has decreased since 2011. AOD during February and particularly March of 2020 were  
230 lower than recent years, but against a noisy background.

231  
232 Figure 4 shows the four retrieved quantities over southern China. There is a springtime maximum in CO (Fig. 4a),  
233 a less regular maximum during September-January, and an annual minimum in July. The range of CO is similar  
234 to central east China. CO over the last 5 years is lower than earlier in the record, and early 2020 CO was higher  
235 than recent years. SO<sub>2</sub> (Fig. 4b) is lower than central east China and any seasonal cycle is also hard to identify.



236 The high June 2011 values are due to the Nabro eruption in Ethiopia (Fromm et al., 2014) which is still apparent  
237 in the time series despite excluding individual SO<sub>2</sub> retrievals that are greater than 15 DU. NO<sub>2</sub> (Fig. 4c) is lower  
238 than over east central China, but both regions share a similar seasonality. NO<sub>2</sub> during January-April 2020 was  
239 slightly lower than 2019. AOD (Fig. 4d) has weak seasonal peaks in October, March and June, has decreased  
240 since 2011, and 2020 fell within the range of 2015-2019.

241

### 242 3.2 East central China

243 Figure 5 shows the distribution of daily CO, SO<sub>2</sub>, NO<sub>2</sub> and AOD for January 23 – April 8 of each year over east  
244 central China. The associated statistics comparing 2020 and 2019 are provided in Table 1, and comparing 2020  
245 with the period over which the trend is consistent in Table 2. The linear trends in each plot start at the year over  
246 which the trend explains most of the variability in the data, which will vary by region and variable. The daily  
247 distribution of AIRS CO (Fig. 5a) is shown by the black box and whisker plots. The variation during January 23  
248 – April 8 of each year is due to weather-related factors and observational error. The mean CO of 133.5 ppbv in  
249 2020 was 3% less than the 2019 mean of 137.9 ppbv, and 12% less than 2005-2019 mean of 150.9 ppbv. The  
250 2020 difference from 2019 is only marginally significant, with a 95% confidence interval (-6% - 0%) close to  
251 spanning 0. The 2020 difference from the 2005-2019 background is significant (-14% - -9%), but during this  
252 period CO declined by -1.8 ppbv yr<sup>-1</sup>, indicated by the red points. This overall decrease includes periods where  
253 CO may have increased, for example from 2010-2012, 2016 and slightly in 2019. Based on this trend, the expected  
254 value for 2020 was 136.8 ppbv (shown in blue). The observed 2020 mean was 2% less than expected, but because  
255 the 95% confidence intervals (-5% - 1%) span 0, this difference is not considered to be significant.

256

257 OMI SO<sub>2</sub> (Fig. 5b) fluctuated over 2005 to 2011 and declined steadily afterward by -.056 DU yr<sup>-1</sup> from 2012-  
258 2019 over east central China. This trend explained 32% of the variation in the data over this period, during which  
259 overall variation declined, becoming narrower to a degree not seen in the CO. Declines were steady, although  
260 2019 may have departed upward from this trend. The 2020 mean of 0.057 was 93% higher than the 2019 mean of  
261 0.032, but with a wide 95% confidence interval (16% - 236%). 2020 SO<sub>2</sub> was 72% lower than the 2012-2019  
262 mean, and with a narrower (-78% - -65%) confidence interval. The observed 2020 SO<sub>2</sub> was 201% higher than the  
263 expected value of -0.06. The change in 2020 SO<sub>2</sub> was strongly dependent on whether daily values were calculated  
264 from the mean or median of individual values over the region. When the median of individual retrievals is used,  
265 2020 was only 8.4% higher than predicted from the 2012-2019 trend (Figure S1b). This likely reflects the greater  
266 influence of high individual retrieval values on the daily mean value compared to the median, even after the basic  
267 filtering of transient SO<sub>2</sub> plumes.

268

269 OMI NO<sub>2</sub> (Fig. 5c) increased from 2005 to 2011 and decreased by  $-0.7 \times 10^{15}$  molec cm<sup>-2</sup> yr<sup>-1</sup> from 2011-2020. The  
270 2020 mean NO<sub>2</sub> of  $6.5 \times 10^{15}$  molec cm<sup>-2</sup> was 32% less than the 2019 mean of  $9.6 \times 10^{15}$  molec cm<sup>-2</sup>, and 43% less  
271 than the 2011-2019 mean of  $11.3 \times 10^{15}$  molec cm<sup>-2</sup>. The pronounced regional difference between 2020 and 2019  
272 (Fig. 2c) in part likely reflects an upward departure in 2019 from the overall trend since 2011. The observed 2020  
273 mean was 17% less than the expected value of  $7.8 \times 10^{15}$  molec cm<sup>-2</sup>, with a wide but negative 95% confidence  
274 interval (-28% - -5%), suggesting that 2020 NO<sub>2</sub> was significantly lower than would be expected from the trend.



275

276 MODIS AOD (Fig. 5d) was flat or slightly increasing from 2005 to 2011 and subsequently changed by  $-0.03 \text{ yr}^{-1}$ .  
277 <sup>1</sup>. The 2020 mean AOD of 0.41 was 15% less than the 2019 mean of 0.48 and 30% less than the 2011-2019  
278 average of 0.58. The observed 2020 mean was 2% higher than the predicted value of 0.40, but with a wide (-15%  
279 - 20%) confidence interval spanning 0, suggesting 2020 was not significantly different from expected.

280

281 In evaluating the 2020 changes, the background period was defined by the period during which the trend was  
282 strongest, using the  $r^2$  value of the trend. This is a reasonable but ad-hoc way of defining a period with consistent  
283 increasing or decreasing trends. Figure 6 shows how the trends and differences between observed and predicted  
284 2020 means depended on the year chosen as the start of the period over which the trend is estimated. AIRS CO  
285 (Fig. 6a) showed uneven changes in the trend (red line) with starting year, and more uncertainty in the trend (red  
286 shading) for later years due to fewer data used for the estimate, but for all years was significantly negative. The  
287 difference between observed 2020 mean and the value predicted from the trend (magenta line) varied inversely  
288 with the trend and was always negative, but, except for 2009, had 95% confidence intervals (magenta shading)  
289 spanning 0, and therefore were not considered significant. The SO<sub>2</sub> trends (Fig. 6b) were all significantly negative.  
290 For trends starting in 2007 and after, the observed 2020 mean was significantly higher than predicted, but these  
291 differences were not consistently significant when daily values were calculated from the median of individual  
292 retrievals (Figure S2b). Earlier starting years produce weaker overall trends in NO<sub>2</sub> (Fig. 6c) because of the NO<sub>2</sub>  
293 increase until 2011, but observed 2020 NO<sub>2</sub> was significantly less than predicted regardless of the starting year.  
294 Note that analyses of SO<sub>2</sub> and NO<sub>2</sub> that include years prior to 2012 may be affected by changes in observation  
295 sample size due to changes in the OMI row anomaly. For AOD (Fig. 6d), there was no significant difference  
296 between the observed and predicted 2020 mean for periods beginning in 2009 and later, when the trends were  
297 strongest.

### 298 3.3 Southern China

299 Figure 7 shows the distribution of daily CO, SO<sub>2</sub>, NO<sub>2</sub> and AOD for January 23-April 8 of each year over southern  
300 China, along with linear trends. The associated statistics comparing 2020 and 2019 are provided in Table 3, and  
301 comparing 2020 with the period over which the trend is consistent in Table 4. For AIRS CO (Fig. 7a), the strongest  
302 trend started in 2007 and was  $-1.8 \text{ ppbv yr}^{-1}$  through 2019. CO in 2020 was 144.8 ppbv, 13% higher than the 2019  
303 mean of 128.4 ppbv which can be seen in an upward shift in the distribution of the box plot, and nearly identical  
304 to the 2007-2019 background period mean of 144.9 ppbv. 2020 CO was 10% higher than predicted from the 2007-  
305 2019 trend, and with 95% confidence interval (5% - 15%) not spanning 0.

306

307 OMI SO<sub>2</sub> (Fig. 7b) changed by  $-0.012 \text{ DU yr}^{-1}$  beginning in 2007, which is driven by fewer high individual SO<sub>2</sub>  
308 values in later years, as in east central China. The 2020 mean of 0.003 DU was 115% higher than the 2019 mean  
309 of  $-0.023 \text{ DU}$  with a wide but positive 95% confidence interval (32% - 215%), and 95% less than the 2007-2019  
310 mean of 0.058 DU. The observed 2020 mean was 109% higher than the predicted value of  $-0.034 \text{ DU}$ , with a wide  
311 but positive 95% confidence interval (54% - 164%).

312



313 OMI NO<sub>2</sub> (Fig. 7c) changed by  $-0.3 \times 10^{15}$  molec cm<sup>-2</sup> yr<sup>-1</sup> beginning in 2011. The 2020 mean of  $3.3 \times 10^{15}$  molec  
314 cm<sup>-2</sup> was 22% less than 2019 and 32% less than 2011-2019, with both differences significant. The 2020 mean was  
315 7% less than the predicted value of  $3.6 \times 10^{15}$  molec cm<sup>-2</sup>, but with a wide 95% confidence interval (-20% - 8%)  
316 spanning 0.

317

318 MODIS AOD (Fig. 7d) changed by  $-0.04$  yr<sup>-1</sup> between 2011 and 2019. The 2020 mean AOD of 0.38 was 12%  
319 higher than the 2019 mean of 0.34, but with a 95% confidence interval (-6% - 32%) spanning 0. 2020 AOD was  
320 17% less than the 2011-2019 mean of 0.46, but 39% higher than predicted from the trend over this period, and  
321 with a wide but positive 95% confidence interval (16% - 65%).

322

323 Figure 8 shows the dependence of the trends and 2020 differences from background period to the starting year  
324 over southern China. AIRS CO (Fig. 8a) had a significant decreasing trend for all starting years, and regardless  
325 of the start year, 2020 was significantly higher than predicted from the trend. SO<sub>2</sub> trends were also negative, and  
326 varied similarly to the CO. The 2020 SO<sub>2</sub> was higher than the background period, but with marginal significance,  
327 given that the confidence intervals spanned 0 for later starting years, and because the differences were not  
328 significant when daily values were calculated from the median SO<sub>2</sub> of individual retrievals for trends starting in  
329 2008 (Figure S3b) or any other year (Figure S4b). NO<sub>2</sub> trends (Fig. 8c) were more strongly decreasing for periods  
330 beginning between 2009 and 2012 and were flat or positive otherwise. The 2020 NO<sub>2</sub> mean was significantly  
331 lower than predicted, except for when the trend was estimated beginning in 2011, when it was the strongest. The  
332 AOD trends varied similarly to the NO<sub>2</sub> but were significantly negative for all start years. The 2020 mean was  
333 significantly higher than predicted for all starting between 2010 and 2015.

334

335 For both regions and all quantities, the differences between observed and predicted values for 2020 were  
336 insensitive to a longer or shorter lockdown period, or to whether the bootstrap resampling was weighted by the  
337 number of valid retrievals each day.

#### 338 4 Discussion and conclusions

339 The degree to which the COVID-19 lockdowns in China resulted in changes in atmospheric composition depends  
340 strongly on whether existing trends are taken into account, and only in certain cases could be considered  
341 significant. For AIRS CO over central east China, the 2020 mean was 12% less than that over 2005-2019, but  
342 only 2% less than what would be expected given the steady decreases over that period, and this 2% was not  
343 significant given the variability of the daily data. Similarly for MODIS AOD, the 2020 mean was 30% less than  
344 over 2011-2019, but no different than what would be expected from trends. SO<sub>2</sub> in 2020 was 72% less than over  
345 2012-2019 but was 201% higher than what would be expected from trends. Daily SO<sub>2</sub> calculated from the mean  
346 of individual retrievals are sensitive to outlying SO<sub>2</sub> values from transient plumes, and when daily SO<sub>2</sub> was  
347 calculated instead from the median across individual retrievals, 2020 SO<sub>2</sub> was only 8% higher than what would  
348 be expected, but still significantly.

349

350 OMI NO<sub>2</sub> in 2020 over central east China was 43% less than over 2011-2019, but only 17% less than what would  
351 be expected from trends. This difference was statistically significant but does suggest that more than half of the



352 reductions in NO<sub>2</sub> in 2020 could be expected independent of COVID-19 lockdowns. For reference, Bauwens et  
353 al. (2020) reported a ~40% drop in OMI NO<sub>2</sub> from 2019 to 2020 over cities affected by the lockdown using the  
354 QA4ECV retrieval (Boersma et al., 2018), and a ~51% drop in NO<sub>2</sub> over the eight cities (Beijing, Jinan, Nanjing,  
355 Qingdao, Tianjin, Wuhan, Xi'an and Zhengzhou) falling within our central east China region. Our analysis cannot  
356 be compared directly because we include non-urban areas and define our lockdown period differently, but we can  
357 say that a large part of the reduction in that study is likely due to background trends, rather than to COVID-19  
358 lockdowns.

359

360 The lack of any significant departure from recent trends in CO and AOD over central east China was unexpected,  
361 given its high population density and level of industrial activity. In the case of MODIS AOD, the lack of an  
362 observable lockdown effect was possibly due to contributions from other sources unaffected by COVID-19 related  
363 lockdowns, limitations in the MODIS AOD retrieval under cloudy conditions, climatological variability from  
364 other sources such as mineral dust, and meteorology favorable to secondary aerosol formation which could have  
365 offset lower emissions (Wang et al., 2020). The 2020 increase in SO<sub>2</sub> is more difficult to interpret because of the  
366 discrepancies between daily values calculated from the mean or median of individual retrievals, but is broadly  
367 consistent with surface observations that find no significant change in in-situ surface SO<sub>2</sub> over Wuhan in the daily  
368 mean, and a slight increase in daytime SO<sub>2</sub> possibly associated with increased residential heating and cooking  
369 (Shi and Brasseur, 2020).

370

371 Over southern China, retrieved SO<sub>2</sub>, NO<sub>2</sub> and AOD were significantly lower in 2020 compared to recent averages.  
372 SO<sub>2</sub> was 95% less than the 2007-2019 mean, but 109% greater than what would be expected from trends. Similarly  
373 to central east China, SO<sub>2</sub> was only 5% higher than expected when daily values were calculated from the median  
374 of individual retrievals, rather than the mean. NO<sub>2</sub> in 2020 was 32% less than over 2011-2019, but only 7% less  
375 than what would be expected from trends, and this difference was not consistently significant for different trend  
376 periods. The more significant reductions in NO<sub>2</sub> in east central China compared to the south is consistent with  
377 Chen et al.'s (2020) detection of a larger 2020 decrease in surface NO<sub>2</sub> in Wuhan compared to Shanghai. Retrieved  
378 CO in 2020 was nearly identical to the 2007-2019 mean, but 10% higher than what would be expected given the  
379 decreasing trend over this period. AOD in 2020 was 17% less than over 2011-2019, but 39% higher than what  
380 would be expected from the trend.

381

382 The focus of this analysis is on whether satellite retrievals of atmospheric composition over 2020 departed  
383 significantly from different background periods and expected values for 2020 when daily variability and trends  
384 are accounted for, but it is useful at a preliminary stage to speculate as to how different emissions changes could  
385 have contributed to 1) why NO<sub>2</sub> was robustly lower in 2020 over east central China compared to CO and AOD,  
386 and 2) why CO and AOD were higher over southern China compared to what would be expected from recent  
387 trends.

388

389 To understand why NO<sub>2</sub> differences over east central China were more significant than other quantities, Table 5  
390 shows the emissions by sector for a representative set of constituents from the Community Emissions Data System  
391 (CEDS) (Hoesly et al., 2018) over China for 2014, the most recent year available. Other bottom-up emissions



392 inventories will vary in absolute emissions amounts and their sector contributions, particularly for more recent  
393 periods, but CEDS is the standard available emissions dataset available globally as a baseline for the next IPCC  
394 assessment, in anticipation of assessing 2020 COVID-19 related changes to atmospheric composition in other  
395 regions, and for modeling studies involving a transboundary transport component. Across all species, energy  
396 production, industrial activity, transportation, residential/commercial/other (RCO), and waste disposal constitute  
397 the bulk of the emissions. Based on activity data for the first quarter of 2020, energy demand across China declined  
398 by 7% compared to 2019, and transportation sector activity declined by 50 to 75% in regions with lockdowns in  
399 place (International Energy Agency, 2020). These sectors are direct or indirect sources of numerous pollutants,  
400 including SO<sub>2</sub> (the precursor of sulfate aerosol), NO<sub>x</sub>, CO, and primary anthropogenic aerosols classified broadly  
401 as organic carbon (OC) and black carbon (BC). If we apply the 7% reduction in energy production and mid-point  
402 62.5% reduction to transportation from the IEA, assume a 20% reduction in industrial emissions, 5% reduction in  
403 waste emissions, no change in RCO (with commercial decreases offset by residential increases), this yields a 10%  
404 reduction in BC, 5% reduction in OC, 14% reduction in SO<sub>2</sub>, 14% reduction in CO and 21% reduction in NO<sub>2</sub>.  
405 The larger reduction in NO<sub>2</sub> relative to other emissions could partly explain why OMI NO<sub>2</sub> column density  
406 changes over central east China were stronger than in the other retrievals.

407

408 Following Si et al.'s (2019) consideration of biomass burning as a pollution source in China alongside  
409 anthropogenic sources, we considered transboundary smoke transport as a possible reason for the higher 2020 CO  
410 over southern China, guided by higher CO over the Upper Mekong region in 2020 compared to 2019 (Fig. 2a).  
411 Table 6 compares January 23-April 8 AIRS CO over southern China to CO emissions estimates from biomass  
412 burning from the Global Fire Assimilation System (GFAS) (Kaiser et al., 2012) over the upper Mekong region  
413 (17° N to 25° N, 95° E to 105° E) including parts of eastern Myanmar, northern Thailand, and northern Laos. From  
414 2005 to 2020, variation in GFAS CO over this region explained a moderate (32%) amount of variability in AIRS  
415 CO over southern China, suggesting it as is a non-negligible contributor to variation in CO concentration, and a  
416 contributor to higher CO in 2020. This illustrates that, at a minimum, sources such as biomass burning smoke and  
417 dust that are less affected by COVID-19 related measures will complicate attribution studies. To that end,  
418 modeling studies following Wang et al. (2020) will be required to isolate emissions, meteorological and chemical  
419 drivers of changes in atmospheric composition and their effects.

420

421 The key implication of our study is that not taking into account past trends in atmospheric composition will lead  
422 to misattribution of changes in air quality to COVID-19 lockdowns. We have approached the issue by comparing  
423 data for 2020 to what would have been expected given recent trends, and by applying a single lockdown period  
424 to two large regions. Other studies over China or elsewhere will inevitably use other approaches that more  
425 explicitly account for seasonality and which relate changes in pollution over smaller areas (e.g. single provinces  
426 or states) to region-specific lockdown measures and timing. Regardless of the approach, however, it is important  
427 to consider recent trends and variability. In places where pollution has decreased, not accounting for recent context  
428 will result in over-attribution of changes in pollution to COVID-19. In places where pollution has increased, such  
429 as parts of South Asia, this will result in under-attribution.



430 **Code/data availability:** All code will be made available if the article is accepted for final publication. All source  
431 data are publicly available.

432

433 **Competing interests:** The authors have no competing interests.

434

435 **Author contribution:** All authors conceived of the study. RF, IG and KT conducted the data analysis. RF and  
436 JH prepared the manuscript with contributions from all co-authors.

437



438 **References**

- 439 Bauwens, M., Compornolle, S., Stavrakou, T., Müller, J., van Gent, J., Eskes, H., Levelt, P. F., van der A., R.,  
440 Veeffkind, J. P., Vlietinck, J., Yu, H., and Zehner, C.: Impact of coronavirus outbreak on NO<sub>2</sub> pollution assessed using  
441 TROPOMI and OMI observations, *Geophysical Research Letters*, 2, 0-3, 10.1029/2020GL087978, 2020.
- 442 Boersma, K. F., Eskes, H. J., Richter, A., De Smedt, I., Lorente, A., Beirle, S., van Geffen, J., Zara, M., Peters, E.,  
443 Van Roozendaal, M., Wagner, T., Maasakkers, J. D., van der A, R. J., Nightingale, J., De Rudder, A., Irie, H., Pinardi,  
444 G., Lambert, J. C., and Compornolle, S. C.: Improving algorithms and uncertainty estimates for satellite NO<sub>2</sub>  
445 retrievals: results from the quality assurance for the essential climate variables (QA4ECV) project, *Atmospheric  
446 Measurement Techniques*, 11, 6651-6678, 10.5194/amt-11-6651-2018, 2018.
- 447 Castellanos, P., Boersma, K. F., Torres, O., and de Haan, J. F.: OMI tropospheric NO<sub>2</sub> air mass factors over South  
448 America: effects of biomass burning aerosols, *Atmospheric Measurement Techniques*, 8, 3831-3849, 10.5194/amt-8-  
449 3831-2015, 2015.
- 450 Chen, K., Wang, M., Huang, C., Kinney, P. L., and Paul, A. T.: Air Pollution Reduction and Mortality Benefit during  
451 the COVID-19 Outbreak in China, *Lancet Planetary Health*, 0-3, 10.1101/2020.03.23.20039842, 2020.
- 452 Chimot, J., Vlemmix, T., Veeffkind, J. P., de Haan, J. F., and Levelt, P. F.: Impact of aerosols on the OMI tropospheric  
453 NO<sub>2</sub> retrievals over industrialized regions: how accurate is the aerosol correction of cloud-free scenes via a simple  
454 cloud model?, *Atmospheric Measurement Techniques*, 9, 359-382, 10.5194/amt-9-359-2016, 2016.
- 455 Efron, B., and Gong, G.: A Leisurely Look at the Bootstrap, the Jackknife, and Cross-Validation, *American Statistician*,  
456 37, 36-48, 10.2307/2685844, 1983.
- 457 Filonchik, M., Yan, H. W., and Zhang, Z. R.: Analysis of spatial and temporal variability of aerosol optical depth  
458 over China using MODIS combined Dark Target and Deep Blue product, *Theoretical and Applied Climatology*, 137,  
459 2271-2288, 10.1007/s00704-018-2737-5, 2019.
- 460 Fioletov, V. E., McLinden, C. A., Krotkov, N., Li, C., Joiner, J., Theys, N., Carn, S., and Moran, M. D.: A global  
461 catalogue of large SO<sub>2</sub> sources and emissions derived from the Ozone Monitoring Instrument, *Atmospheric Chemistry  
462 and Physics*, 16, 11497-11519, 10.5194/acp-16-11497-2016, 2016.
- 463 Fromm, M., Kablick, G., Nedoluha, G., Carboni, E., Grainger, R., Campbell, J., and Lewis, J.: Correcting the record  
464 of volcanic stratospheric aerosol impact: Nabro and Sarychev Peak, *Journal of Geophysical Research-Atmospheres*,  
465 119, 10.1002/2014jd021507, 2014.
- 466 Geddes, J. A., Martin, R. V., Boys, B. L., and van Donkelaar, A.: Long-Term Trends Worldwide in Ambient NO<sub>2</sub>  
467 Concentrations Inferred from Satellite Observations, *Environmental Health Perspectives*, 124, 281-289,  
468 10.1289/ehp.1409567, 2016.
- 469 Georgoulias, A. K., van der A, R. J., Stammes, P., Boersma, K. F., & Eskes, H. J.: Trends and trend reversal detection  
470 in two decades of tropospheric NO<sub>2</sub> satellite observations, *Atmospheric Chemistry and Physics*, 19, 6269-6294,  
471 <https://doi.org/10.5194/acp-2018-988>, 2019.
- 472 Han, H., Liu, J., Yuan, H. L., Jiang, F., Zhu, Y., Wu, Y., Wang, T. J., and Zhuang, B. L.: Impacts of Synoptic Weather  
473 Patterns and their Persistency on Free Tropospheric Carbon Monoxide Concentrations and Outflow in Eastern China,  
474 *Journal of Geophysical Research-Atmospheres*, 123, 7024-7046, 10.1029/2017jd028172, 2018.



- 475 He, Q. Q., Gu, Y. F., and Zhang, M.: Spatiotemporal patterns of aerosol optical depth throughout China from 2003 to  
476 2016, *Science of the Total Environment*, 653, 23-35, 10.1016/j.scitotenv.2018.10.307, 2019.
- 477 Hoesly, R. M., Smith, S. J., Feng, L. Y., Klimont, Z., Janssens-Maenhout, G., Pitkanen, T., Seibert, J. J., Vu, L.,  
478 Andres, R. J., Bolt, R. M., Bond, T. C., Dawidowski, L., Kholod, N., Kurokawa, J., Li, M., Liu, L., Lu, Z. F., Moura,  
479 M. C. P., O'Rourke, P. R., and Zhang, Q.: Historical (1750-2014) anthropogenic emissions of reactive gases and  
480 aerosols from the Community Emissions Data System (CEDS), *Geoscientific Model Development*, 11, 369-408,  
481 10.5194/gmd-11-369-2018, 2018.
- 482 Hubanks, P., Platnick, S., King, M., and Ridgway, B.: MODIS Algorithm Theoretical Basis Document No. ATBD-  
483 MOD-30 for Level-3 Global Gridded Atmosphere Products (08\_D3, 08\_E3, 08\_M3) and Users Guide (Collection 6.0  
484 & 6.1, Version 4.4, 20 Feb 2019), NASA Goddard Space Flight Center, Greenbelt, MD, 2019.
- 485 Kaiser, J. W., Heil, A., Andreae, M. O., Benedetti, A., Chubarova, N., Jones, L., Morcrette, J. J., Razinger, M., Schultz,  
486 M. G., Suttie, M., and van der Werf, G. R.: Biomass burning emissions estimated with a global fire assimilation system  
487 based on observed fire radiative power, *Biogeosciences*, 9, 527-554, 10.5194/bg-9-527-2012, 2012.
- 488 Krotkov, N. A.: OMI/Aura NO<sub>2</sub> Cloud-Screened Total and Tropospheric Column L3 Global Gridded 0.25 degree x  
489 0.25 degree V3, NASA Goddard Space Flight Center, 2013.
- 490 Krotkov, N. A., McLinden, C. A., Li, C., Lamsal, L. N., Celarier, E. A., Marchenko, S. V., Swartz, W. H., Bucsela,  
491 E. J., Joiner, J., Duncan, B. N., Boersma, K. F., Veeffkind, J. P., Levelt, P. F., Fioletov, V. E., Dickerson, R. R., He,  
492 H., Lu, Z., and Streets, D. G.: Aura OMI observations of regional SO<sub>2</sub> and NO<sub>2</sub> pollution changes from 2005 to 2015,  
493 *Atmospheric Chemistry and Physics*, 16, 4605-4629, 10.5194/acp-16-4605-2016, 2016.
- 494 Krotkov, N. A., Lamsal, L. N., Celarier, E. A., Swartz, W. H., Marchenko, S. V., Bucsela, E. J., Chan, K. L., Wenig,  
495 M., and Zara, M.: The version 3 OMI NO<sub>2</sub> standard product, *Atmospheric Measurement Techniques*, 10, 3133-3149,  
496 10.5194/amt-10-3133-2017, 2017.
- 497 Lamsal, L. N., Krotkov, N. A., Celarier, E. A., Swartz, W. H., Pickering, K. E., Bucsela, E. J., Gleason, J. F., Martin,  
498 R. V., Philip, S., Irie, H., Cede, A., Herman, J., Weinheimer, A., Szykman, J. J., and Knepp, T. N.: Evaluation of OMI  
499 operational standard NO<sub>2</sub> column retrievals using in situ and surface-based NO<sub>2</sub> observations, *Atmospheric  
500 Chemistry and Physics*, 14, 11587-11609, 10.5194/acp-14-11587-2014, 2014.
- 501 Levy, R. C., Remer, L. A., Kleidman, R. G., Mattoo, S., Ichoku, C., Kahn, R., and Eck, T. F.: Global evaluation of  
502 the Collection 5 MODIS dark-target aerosol products over land, *Atmospheric Chemistry and Physics*, 10, 10399-  
503 10420, 10.5194/acp-10-10399-2010, 2010.
- 504 Li, C., Joiner, J., Krotkov, N. A., and Bhartia, P. K.: A fast and sensitive new satellite SO<sub>2</sub> retrieval algorithm based  
505 on principal component analysis: Application to the ozone monitoring instrument, *Geophysical Research Letters*, 40,  
506 6314-6318, 10.1002/2013gl058134, 2013.
- 507 Li, M., Zhang, Q., Kurokawa, J., Woo, J. H., He, K. B., Lu, Z. F., Ohara, T., Song, Y., Streets, D. G., Carmichael, G.  
508 R., Cheng, Y. F., Hong, C. P., Huo, H., Jiang, X. J., Kang, S. C., Liu, F., Su, H., and Zheng, B.: MIX: a mosaic Asian  
509 anthropogenic emission inventory under the international collaboration framework of the MICS-Asia and HTAP,  
510 *Atmospheric Chemistry and Physics*, 17, 935-963, 10.5194/acp-17-935-2017, 2017.
- 511 Lin, C. Q., Liu, G., Lau, A. K. H., Li, Y., Li, C. C., Fung, J. C. H., and Lao, X. Q.: High-resolution satellite remote  
512 sensing of provincial PM<sub>2.5</sub> trends in China from 2001 to 2015. *Atmospheric Environment*, 180, 110-116,  
513 <https://doi.org/10.1016/j.atmosenv.2018.02.045>, 2018.
- 514 Lin, N., Wang, Y. X., Zhang, Y., and Yang, K.: A large decline of tropospheric NO<sub>2</sub> in China observed from space  
515 by SNPP OMPS, *Science of the Total Environment*, 675, 337-342, 10.1016/j.scitotenv.2019.04.090, 2019.



- 516 Luan, Y., and Jaegle, L.: Composite study of aerosol export events from East Asia and North America, *Atmospheric*  
517 *Chemistry and Physics*, 13, 1221-1242, 10.5194/acp-13-1221-2013, 2013.
- 518 Ma, Z. W., Hu, X. F., Sayer, A. M., Levy, R., Zhang, Q., Xue, Y. G., Tong, S. L., Bi, J., Huang, L., and Liu, Y.:  
519 Satellite-Based Spatiotemporal Trends in PM<sub>2.5</sub> Concentrations: China, 2004-2013, *Environmental Health*  
520 *Perspectives*, 124, 184-192, 10.1289/ehp.1409481, 2016.
- 521 McLinden, C. A., Fioletov, V., Boersma, K. F., Kharol, S. K., Krotkov, N., Lamsal, L., Makar, P. A., Martin, R. V.,  
522 Veeffkind, J. P., and Yang, K.: Improved satellite retrievals of NO<sub>2</sub> and SO<sub>2</sub> over the Canadian oil sands and  
523 comparisons with surface measurements, *Atmospheric Chemistry and Physics*, 14, 3637-3656, 10.5194/acp-14-3637-  
524 2014, 2014.
- 525 Mijling, B., van der A, R. J., Boersma, K. F., Van Roozendaal, M., De Smedt, I., and Kelder, H. M.: Reductions of  
526 NO<sub>2</sub> detected from space during the 2008 Beijing Olympic Games, *Geophysical Research Letters*, 36,  
527 10.1029/2009gl038943, 2009.
- 528 Sarkodie, S. A., and Strezov, V.: A review on Environmental Kuznets Curve hypothesis using bibliometric and meta-  
529 analysis, *Science of the Total Environment*, 649, 128-145, 10.1016/j.scitotenv.2018.08.276, 2019.
- 530 Sayer, A. M., Hsu, N. C., Bettenhausen, C., and Jeong, M. J.: Validation and uncertainty estimates for MODIS  
531 Collection 6 "Deep Blue" aerosol data, *Journal of Geophysical Research-Atmospheres*, 118, 7864-7872,  
532 10.1002/jgrd.50600, 2013.
- 533 Sayer, A. M., Munchak, L. A., Hsu, N. C., Levy, R. C., Bettenhausen, C., and Jeong, M. J.: MODIS Collection 6  
534 aerosol products: Comparison between Aqua's e-Deep Blue, Dark Target, and "merged" data sets, and usage  
535 recommendations, *Journal of Geophysical Research-Atmospheres*, 119, 13965-13989, 10.1002/2014jd022453, 2014.
- 536 Schutgens, N., Sayer, A. M., Heckel, A., Hsu, C., Jethva, H., de Leeuw, G., Leonard, P. J. T., Levy, R. C., Lipponen,  
537 A., Lyapustin, A., North, P., Popp, T., Poulson, C., Sawyer, V., Sogacheva, L., Thomas, G., Torres, O., Wang, Y.,  
538 Kinne, S., Schulz, M., and Stier, P.: An AeroCom/AeroSat study: Intercomparison of Satellite AOD Datasets for  
539 Aerosol Model Evaluation, *Atmos. Chem. Phys. Discuss.*, 2020, 1-43, 10.5194/acp-2019-1193, 2020.
- 540 Selden, T. M., and Song, D. Q.: Environmental Quality and Development - is there a Kuznets Curve for Air-Pollution  
541 Emissions?, *Journal of Environmental Economics and Management*, 27, 147-162, 10.1006/jeem.1994.1031, 1994.
- 542 Shah, V., Jacob, D. J., Li, K., Silvern, R. F., Zhai, S. X., Liu, M. Y., Lin, J. T., and Zhang, Q.: Effect of changing NO<sub>x</sub>  
543 lifetime on the seasonality and long-term trends of satellite-observed tropospheric NO<sub>2</sub> columns over China,  
544 *Atmospheric Chemistry and Physics*, 20, 1483-1495, 10.5194/acp-20-1483-2020, 2020.
- 545 Shao, P. Y., Tian, H. Z., Sun, Y. J., Liu, H. J., Wu, B. B., Liu, S. H., Liu, X. Y., Wu, Y. M., Liang, W. Z., Wang, Y.,  
546 Gao, J. J., Xue, Y. F., Bai, X. X., Liu, W., Lin, S. M., and Hu, G. Z.: Characterizing remarkable changes of severe  
547 haze events and chemical compositions in multi-size airborne particles (PM<sub>1</sub>, PM<sub>2.5</sub> and PM<sub>10</sub>) from January 2013  
548 to 2016-2017 winter in Beijing, China, *Atmospheric Environment*, 189, 133-144, 10.1016/j.atmosenv.2018.06.038,  
549 2018.
- 550 Shi, X., and Brasseur, G. P.: The Response in Air Quality to the Reduction of Chinese Economic Activities during the  
551 COVID-19 Outbreak, *Geophysical Research Letters*, 0-1, 10.1029/2020GL088070, 2020.
- 552 Si, Y. D., Wang, H. M., Cai, K., Chen, L. F., Zhou, Z. C., and Li, S. S.: Long-term (2006-2015) variations and relations  
553 of multiple atmospheric pollutants based on multi-remote sensing data over the North China Plain, *Environmental*  
554 *Pollution*, 255, 10.1016/j.envpol.2019.113323, 2019.



- 555 Sogacheva, L., Popp, T., Sayer, A. M., Dubovik, O., Garay, M. J., Heckel, A., Hsu, N. C., Jethva, H., Kahn, R. A.,  
556 Kolmonen, P., Kosmala, M., de Leeuw, G., Levy, R. C., Litvinov, P., Lyapustin, A., North, P., Torres, O., and Arola,  
557 A.: Merging regional and global aerosol optical depth records from major available satellite products, *Atmospheric  
558 Chemistry and Physics*, 20, 2031-2056, 10.5194/acp-20-2031-2020, 2020.
- 559 Strode, S. A., Worden, H. M., Damon, M., Douglass, A. R., Duncan, B. N., Emmons, L. K., Lamarque, J.-F., Manyin,  
560 M., Oman, L. D., Rodriguez, J. M., Strahan, S. E., and Tilmes, S.: Interpreting space-based trends in carbon monoxide  
561 with multiple models, *Atmospheric Chemistry and Physics*, 16, 7285-7294, 10.5194/acp-16-7285-2016, 2016.
- 562 Sun, W., Shao, M., Granier, C., Liu, Y., Ye, C. S., and Zheng, J. Y.: Long-Term Trends of Anthropogenic SO<sub>2</sub>, NO<sub>x</sub>,  
563 CO, and NMVOCs Emissions in China, *Earth's Future*, 6, 1112-1133, 10.1029/2018ef000822, 2018.
- 564 United Nations Environment Program (UNEP): Independent Environmental Assessment: Beijing 2008 Olympic  
565 Games. Nairobi, Kenya, 2009.
- 566 Wang, M., Zhu, T., Zheng, J., Zhang, R. Y., Zhang, S. Q., Xie, X. X., Han, Y. Q., and Li, Y.: Use of a mobile laboratory  
567 to evaluate changes in on-road air pollutants during the Beijing 2008 Summer Olympics, *Atmospheric Chemistry and  
568 Physics*, 9, 8247-8263, 10.5194/acp-9-8247-2009, 2009.
- 569 Wang, P., Chen, K., Zhu, S., Wang, P., and Zhang, H.: Severe air pollution events not avoided by reduced  
570 anthropogenic activities during COVID-19 outbreak, *Resources, Conservation and Recycling*, 158, 104814,  
571 10.1016/j.resconrec.2020.104814, 2020.
- 572 Wang, P. C., Elansky, N. F., Timofeev, Y. M., Wang, G. C., Golitsyn, G. S., Makarova, M. V., Rakitin, V. S., Shtabkin,  
573 Y., Skorokhod, A. I., Grechko, E. I., Fokeeva, E. V., Safronov, A. N., Ran, L., and Wang, T.: Long-Term Trends of  
574 Carbon Monoxide Total Columnar Amount in Urban Areas and Background Regions: Ground- and Satellite-based  
575 Spectroscopic Measurements, *Advances in Atmospheric Sciences*, 35, 785-795, 10.1007/s00376-017-6327-8, 2018.
- 576 Wang, T., Nie, W., Gao, J., Xue, L. K., Gao, X. M., Wang, X. F., Qiu, J., Poon, C. N., Meinardi, S., Blake, D., Wang,  
577 S. L., Ding, A. J., Chai, F. H., Zhang, Q. Z., and Wang, W. X.: Air quality during the 2008 Beijing Olympics:  
578 secondary pollutants and regional impact, *Atmospheric Chemistry and Physics*, 10, 7603-7615, 10.5194/acp-10-7603-  
579 2010, 2010.
- 580 Wang, Y., and Wang, J.: Tropospheric SO<sub>2</sub> and NO<sub>2</sub> in 2012-2018: Contrasting views of two sensors (OMI and  
581 OMPS) from space, *Atmospheric Environment*, 223, 10.1016/j.atmosenv.2019.117214, 2020.
- 582 Warner, J., Carminati, F., Wei, Z., Lahoz, W., and Attie, J. L.: Tropospheric carbon monoxide variability from AIRS  
583 under clear and cloudy conditions, *Atmospheric Chemistry and Physics*, 13, 12469-12479, 10.5194/acp-13-12469-  
584 2013, 2013.
- 585 Witte, J. C., Schoeberl, M. R., Douglass, A. R., Gleason, J. F., Krotkov, N. A., Gille, J. C., Pickering, K. E., and  
586 Livesey, N.: Satellite observations of changes in air quality during the 2008 Beijing Olympics and Paralympics,  
587 *Geophysical Research Letters*, 36, 10.1029/2009gl0139236, 2009.
- 588 Xie, G. Q., Wang, M., Pan, J., and Zhu, Y.: Spatio-temporal variations and trends of MODIS C6.1 Dark Target and  
589 Deep Blue merged aerosol optical depth over China during 2000-2017, *Atmospheric Environment*, 214,  
590 10.1016/j.atmosenv.2019.116846, 2019.
- 591 Xu, J. H., Xie, H. M., Wang, K., Wang, J., and Xia, Z. S.: Analyzing the spatial and temporal variations in tropospheric  
592 NO<sub>2</sub> column concentrations over China using multisource satellite remote sensing, *Journal of Applied Remote  
593 Sensing*, 14, 10.1117/1.jrs.14.014519, 2020.



- 594 Yu, S. M., Yuan, J. G., and Liang, X. Y.: Trends and Spatiotemporal Patterns of Tropospheric NO<sub>2</sub> over China During  
595 2005-2014, *Water Air and Soil Pollution*, 228, 10.1007/s11270-017-3641-9, 2017.
- 596 Yumimoto, K., Uno, I., and Itahashi, S.: Long-term inverse modeling of Chinese CO emission from satellite  
597 observations, *Environmental Pollution*, 195, 308-318, 10.1016/j.envpol.2014.07.026, 2014.
- 598 Zhang, Y., Li, C., Krotkov, N. A., Joiner, J., Fioletov, V., and McLinden, C.: Continuation of long-term global SO<sub>2</sub>  
599 pollution monitoring from OMI to OMPS, *Atmospheric Measurement Techniques*, 10, 10.5194/amt-10-1495-2017,  
600 2017.
- 601 Zhao, Y., Nielsen, C. P., McElroy, M. B., Zhang, L., and Zhang, J.: CO emissions in China: Uncertainties and  
602 implications of improved energy efficiency and emission control, *Atmospheric Environment*, 49, 103-113,  
603 10.1016/j.atmosenv.2011.12.015, 2012.
- 604 Zhao, Y., Zhang, J., and Nielsen, C. P.: The effects of recent control policies on trends in emissions of anthropogenic  
605 atmospheric pollutants and CO<sub>2</sub> in China, *Atmospheric Chemistry and Physics*, 13, 487-508, 10.5194/acp-13-487-  
606 2013, 2013.
- 607 Zheng, B., Chevallier, F., Ciais, P., Yin, Y., Deeter, M. N., Worden, H. M., Wang, Y. L., Zhang, Q., and He, K. B.:  
608 Rapid decline in carbon monoxide emissions and export from East Asia between years 2005 and 2016, *Environmental*  
609 *Research Letters*, 13, 10.1088/1748-9326/aab2b3, 2018a.
- 610 Zheng, B., Tong, D., Li, M., Liu, F., Hong, C. P., Geng, G. N., Li, H. Y., Li, X., Peng, L. Q., Qi, J., Yan, L., Zhang,  
611 Y. X., Zhao, H. Y., Zheng, Y. X., He, K. B., and Zhang, Q.: Trends in China's anthropogenic emissions since 2010 as  
612 the consequence of clean air actions, *Atmospheric Chemistry and Physics*, 18, 14095-14111, 10.5194/acp-18-14095-  
613 2018, 2018b.
- 614



615 **Tables**

616

617 **Table 1. Summary statistics for central east China comparing 2020 and 2019 during January 23 – April 8.**

Variable	2020 %		
	2020 mean	2019 mean	difference from 2019
<b>CO</b> (ppbv)	133.5 (130.4, 136.8)	137.9 (134.6, 141.2)	-3 (-6, 0)
<b>SO<sub>2</sub></b> (DU)	0.057 (0.045, 0.070)	0.032 (0.018, 0.046)	93 (16, 236)
<b>NO<sub>2</sub></b> (10 <sup>15</sup> molec cm <sup>-2</sup> )	6.5 (5.7, 7.2)	9.6 (8.7, 10.5)	-32 (-42, -22)
<b>AOD</b>	0.41 (0.36, 0.46)	0.48 (0.41, 0.55)	-15 (-30, 3)

618

619



620 **Table 2. Summary statistics for central east China during January 23 – April 8 over consistent trend periods. The**  
 621 **background start year is that for which estimated trends explained most variability in the daily data through 2019, judging**  
 622 **by the coefficient of determination ( $r^2$ ) of the estimated trend. The background means and trends are estimated from the**  
 623 **background start year through 2019, and the 2020 prediction is calculated from this trend. Numbers in parentheses are**  
 624 **bootstrap-estimated 95% confidence intervals. The trends and percent differences are considered to be significant if their**  
 625 **confidence intervals do not span 0.**

Variable	Background start year	Background mean	2020			2020 predicted from trend	2020 % difference from trend
			Background from background	trend ( $\text{yr}^{-1}$ )	trend $r^2$		
CO (ppbv)	2005	150.9	-12	-1.8	0.17	136.8	-2
		(149.8, 152.1)	(-14, -9)	(-2.0, -1.5)	(0.13, 0.21)	(134.8, 138.8)	(-5, 1)
SO <sub>2</sub> (DU)	2012	0.206	-72	-0.056	0.32	-0.061	201
		(0.184, 0.229)	(-78, -65)	(-0.065, -0.048)	(0.26, 0.38)	(-0.090, -0.033)	(158, 277)
NO <sub>2</sub> (10 <sup>15</sup> molec cm <sup>-2</sup> )	2011	11.3	-43	-0.7	0.17	7.8	-17
		(10.9, 11.7)	(-49, -36)	(-0.8, -0.5)	(0.11, 0.22)	(7.1, 8.5)	(-28, -5)
AOD	2011	0.58	-30	-0.03	0.08	0.4	2
		(0.55, 0.60)	(-39, -20)	(-0.05, -0.02)	(0.04, 0.13)	(0.35, 0.45)	(-15, 20)

626



627 **Table 3. Same as Table 1, but for southern China.**

Variable	2020 %		
	2020 mean	2019 mean	difference from 2019
<b>CO</b> (ppbv)	144.8 (139.4, 150.3)	128.4 (124.1, 132.6)	13 (7, 19)
<b>SO<sub>2</sub></b> (DU)	0.003 (-0.013, 0.019)	-0.023 (-0.039, -0.009)	115 (32, 215)
<b>NO<sub>2</sub></b> (10 <sup>15</sup> molec cm <sup>-2</sup> )	3.3 (3.0, 3.6)	4.3 (3.9, 4.7)	-22 (-32, -10)
<b>AOD</b>	0.38 (0.33, 0.43)	0.34 (0.30, 0.39)	12 (-6, 31)

628



629 **Table 4. Same as Table 2, but for southern China.**

Variable	Background start year	Background mean	2020		trend (yr <sup>-1</sup> )	trend r <sup>2</sup>	2020	2020 %
			difference from background	predicted from trend			difference from trend	
CO (ppbv)	2007	144.9	0	-1.8	0.09	132.1	10	
		(143.3, 146.5)	(-4, 4)	(-2.2, -1.4)	(0.05, 0.13)	(129.5, 134.8)	(5, 15)	
SO <sub>2</sub> (DU)	2007	0.058	-95	-0.012	0.13	-0.034	109	
		(0.049, 0.068)	(-123, -65)	(-0.014, -0.009)	(0.09, 0.17)	(-0.049, -0.019)	(54, 164)	
NO <sub>2</sub> (10 <sup>15</sup> molec cm <sup>-2</sup> )	2011	4.9	-32	-0.3	0.08	3.6	-7	
		(4.7, 5.1)	(-39, -25)	(-0.3, -0.2)	(0.05, 0.13)	(3.2, 3.9)	(-20, 8)	
AOD	2011	0.46	-17	-0.04	0.18	0.27	39	
		(0.44, 0.48)	(-27, -6)	(-0.04, -0.03)	(0.13, 0.23)	(0.24, 0.31)	(16, 65)	

630



631 **Table 5. 2014 anthropogenic emissions estimates by sector (in %) over China, excluding biomass burning, from the**  
632 **Community Emissions Data System (CEDS) for a representative set of constituents: black carbon (BC), carbon monoxide**  
633 **(CO), ammonia (NH<sub>3</sub>), nitrogen oxides (NO<sub>x</sub>), organic carbon (OC) and sulfur dioxide (SO<sub>2</sub>). Residential, commercial and**  
634 **other sectors are combined as RCO.**

	<b>BC</b>	<b>CO</b>	<b>NH<sub>3</sub></b>	<b>NO<sub>x</sub></b>	<b>OC</b>	<b>SO<sub>2</sub></b>
Agriculture	0	0	61.6	1.1	0	0
Energy	32.6	8	0.4	38.5	28.3	29.4
Industrial	12.7	41.8	6.5	33	5.1	57.3
Ground transportation	8.1	7.2	0.5	17.5	1.7	0.3
RCO	38.1	36.7	5.2	4.2	38.4	12.5
Solvents	0	0	0	0	0	0
Waste	8.5	6.3	25.8	5.2	26.5	0.4
Shipping	0	0	0	0.2	0	0.1
Aircraft	0	0	0	0.2	0	0

635



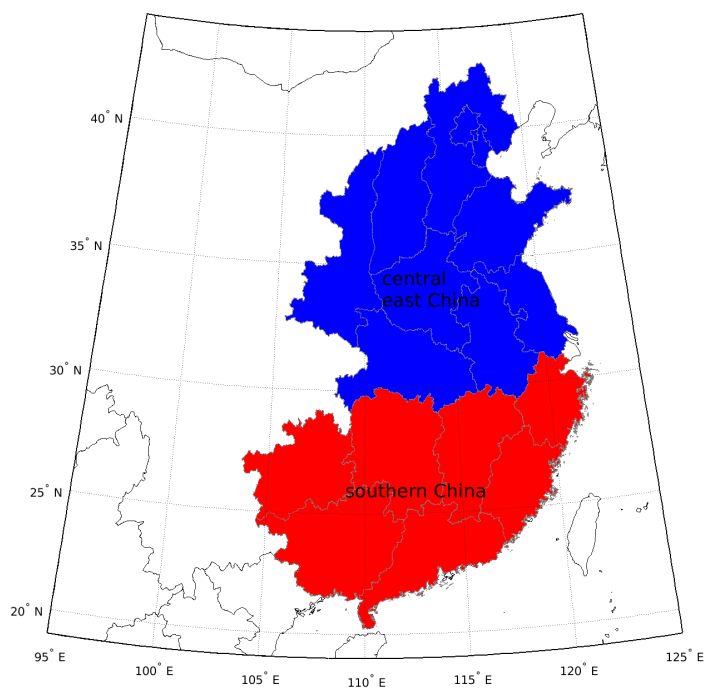
636 **Table 6. Bottom up biomass Global Fire Assimilation System (Kaiser et al., 2012) burning CO emissions estimates from the**  
637 **Upper Mekong region (17° N to 24° N, 95° E to 105° E) and AIRS CO over southern China from January 23 to April 8, for**  
638 **2005-2020.**

Year	GFAS CO	AIRS CO
	Upper Mekong (KT)	southern China 500 hPa (ppbv)
2005	7977	157
2006	8905	146
2007	15734	165
2008	4542	153
2009	9990	140
2010	14176	149
2011	3591	147
2012	11320	153
2013	8684	145
2014	8722	142
2015	8084	143
2016	9642	149
2017	3736	131
2018	3179	139
2019	6309	128
2020	7871	145

639

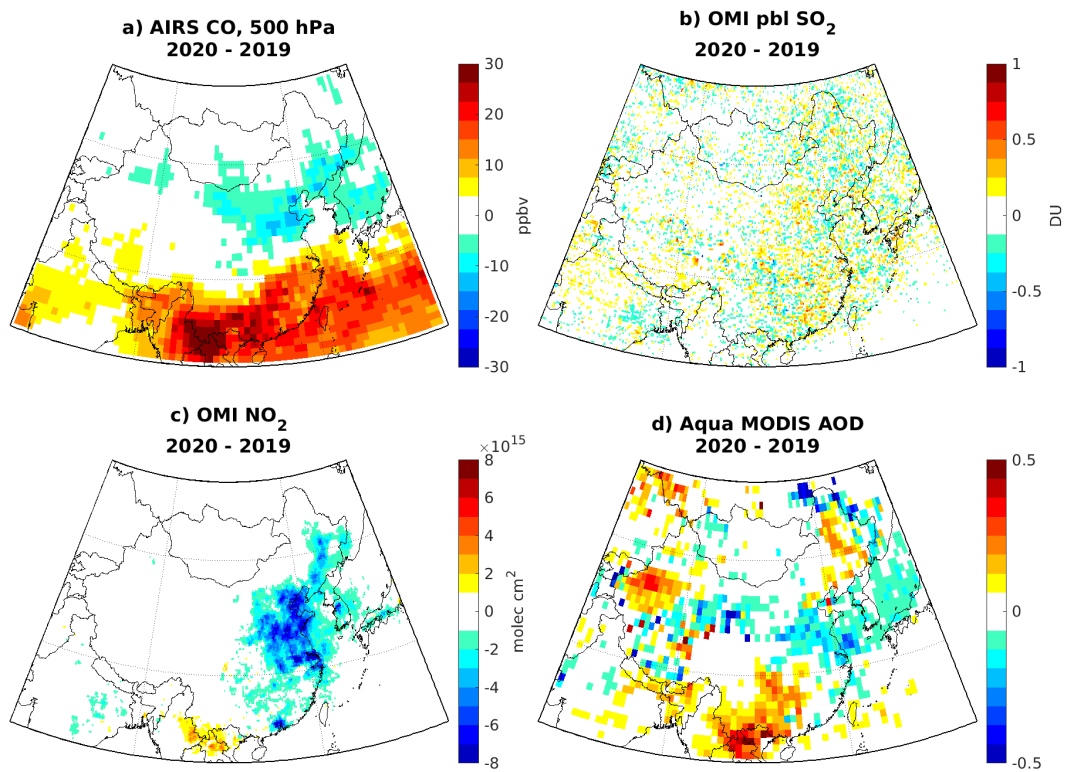


640 **Figures**



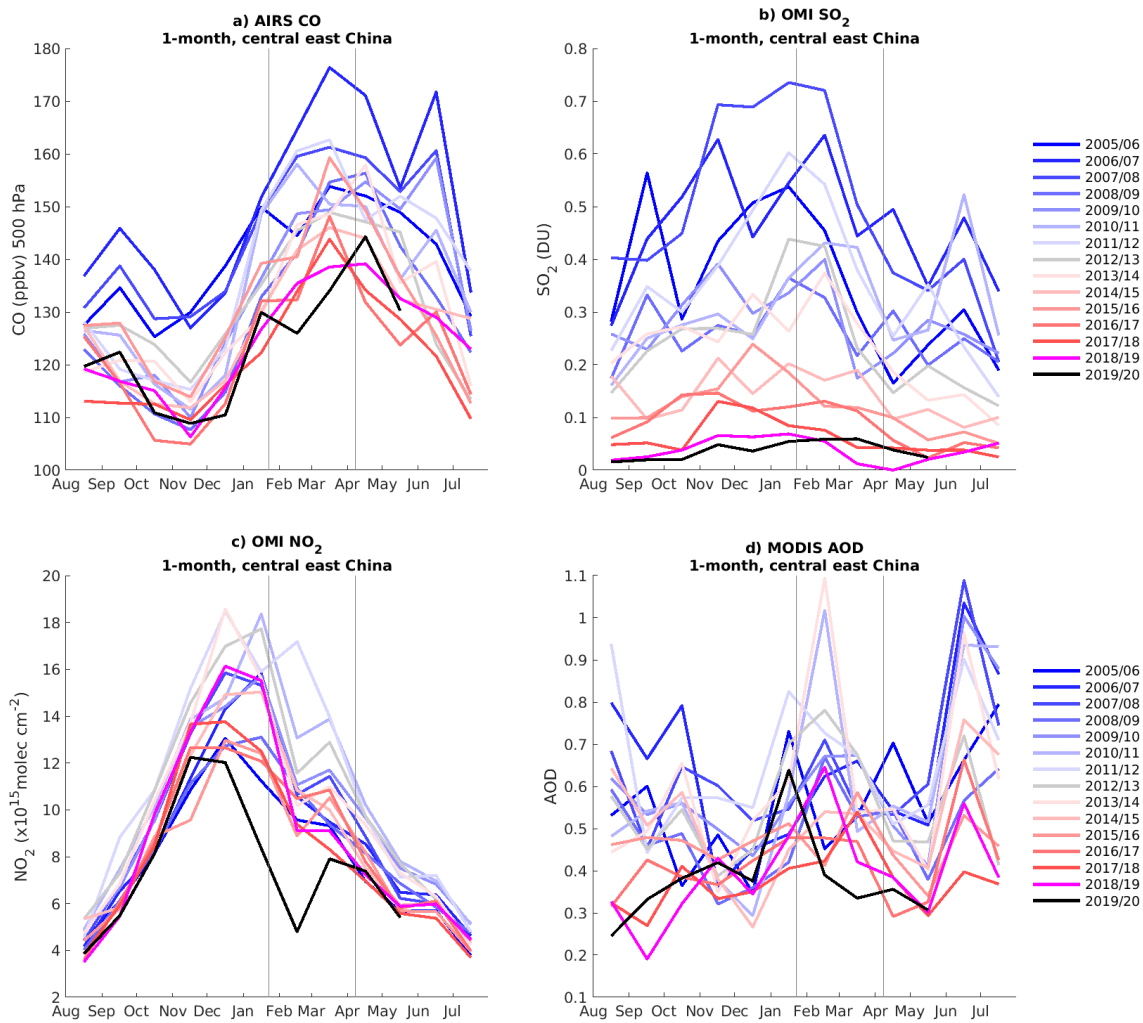
641

642 **Figure 1. Groupings of provinces for central east China and southern China.**



643

644 **Figure 2.** 2020-2019 differences during January 23 to April 8 over China in a) AIRS carbon monoxide (CO) at 500 hPa, b)  
645 OMI PBL sulfur dioxide (SO<sub>2</sub>), c) OMI tropospheric nitrogen dioxide (NO<sub>2</sub>) and d) Aqua MODIS aerosol optical depth  
646 (AOD).



650 **Figure 3.** Monthly mean a) AIRS CO, b) OMI PBL SO<sub>2</sub>, c) OMI tropospheric NO<sub>2</sub> and d) MODIS AOD over central east China since 2005. As in Bauwens et al. (2020), each year starts in August to show any departure from the seasonal cycle during the January 23 to April 8 lockdown period, shown by the thin grey vertical lines.

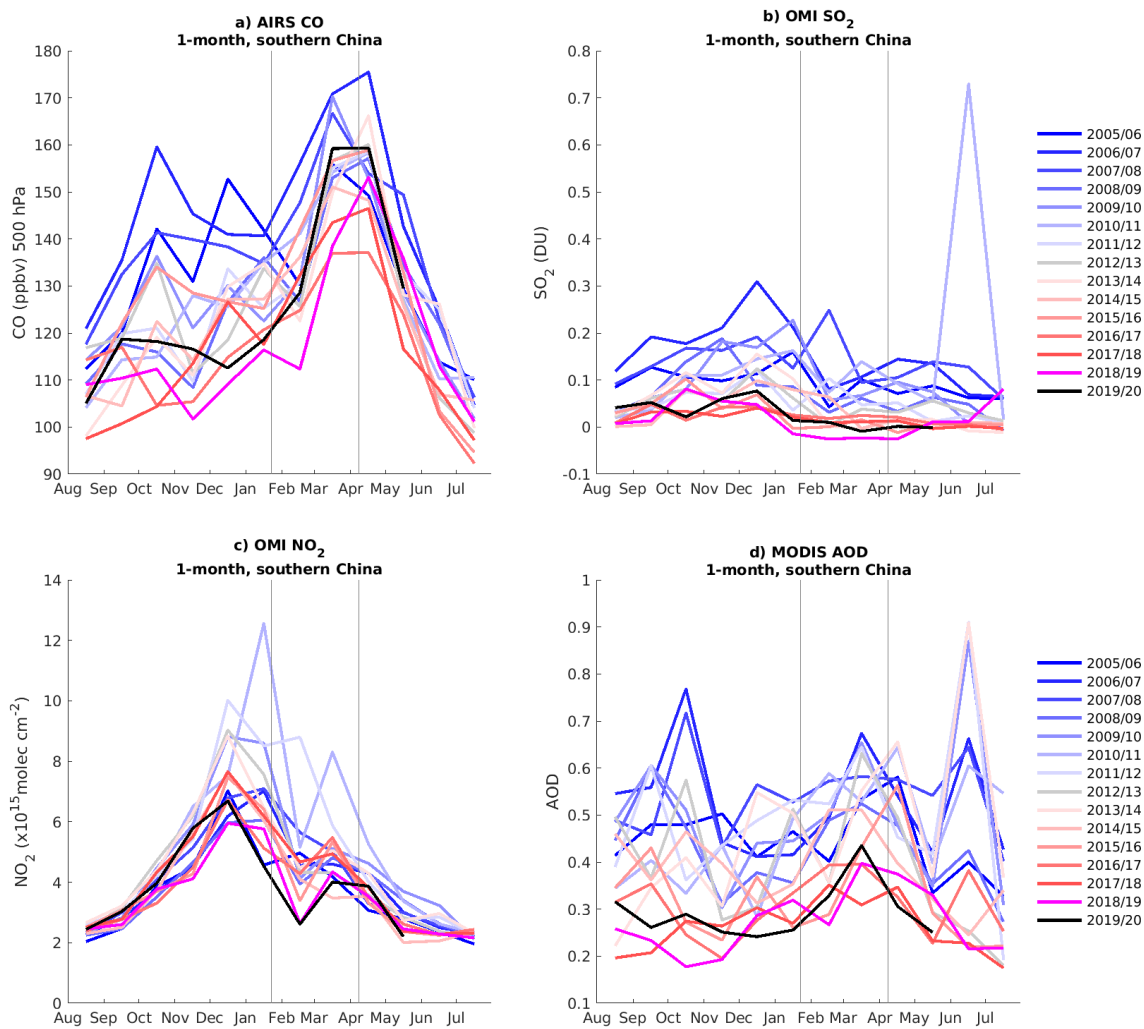
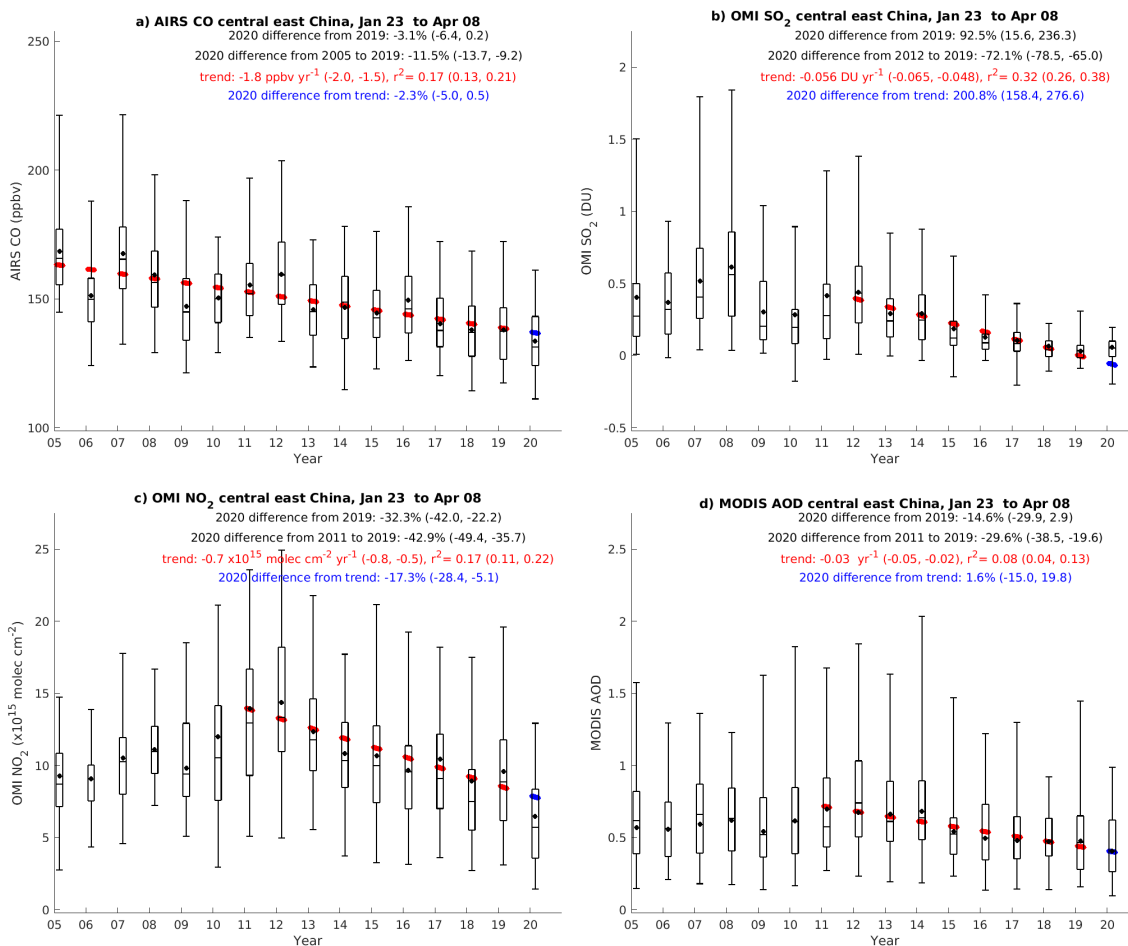
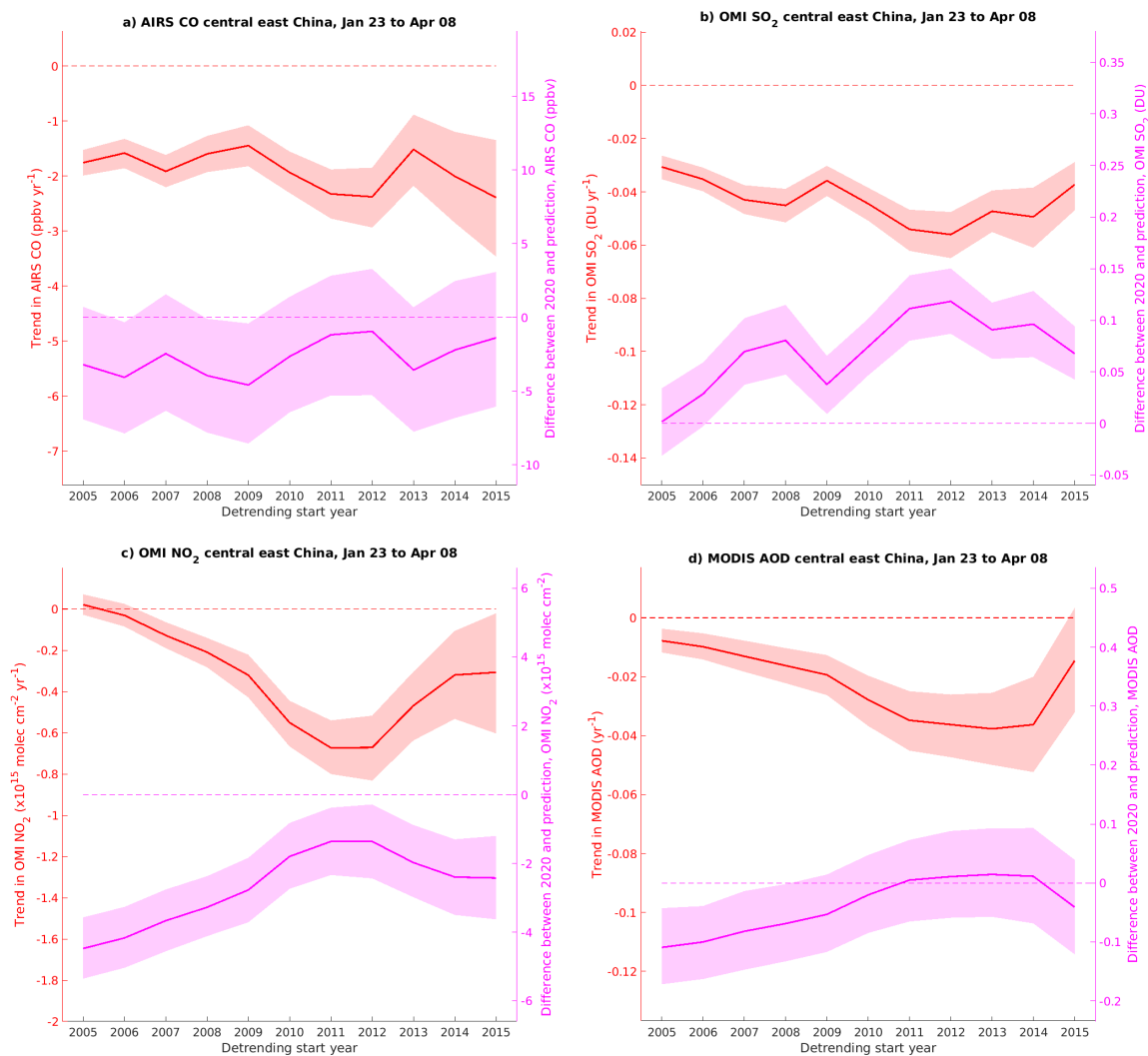


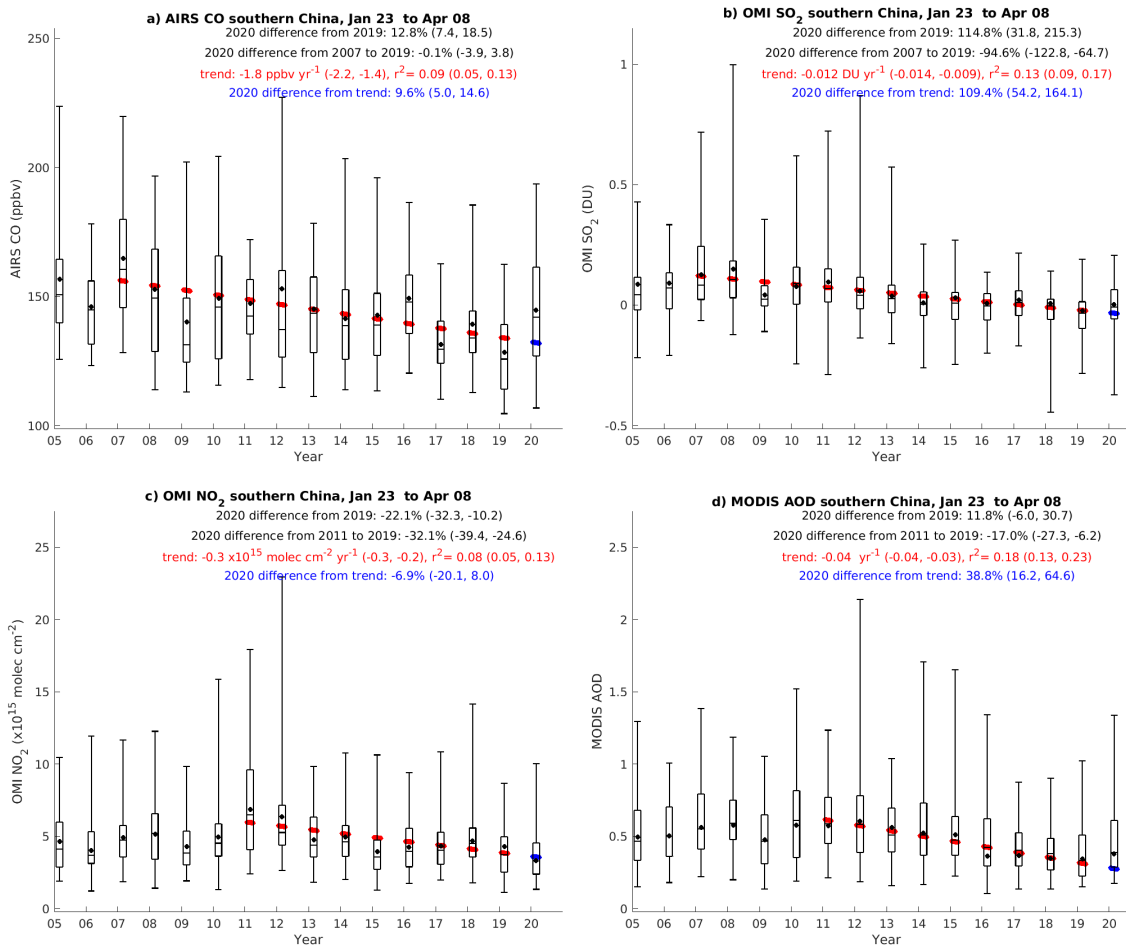
Figure 4. Same as Figure 3, but for southern China.



655 Figure 5. January 23–April 8 box plots over central East China for a) AIRS CO, b) OMI PBL SO<sub>2</sub>, c) OMI tropospheric NO<sub>2</sub> and d)  
 Aqua and Terra MODIS AOD from 2005 to 2020. The black box plots show the median, interquartile range and 2.5<sup>th</sup> and 97.5<sup>th</sup>  
 percentiles over all daily mean data. For each variable, the estimated trend is plotted in red over the period during which it was  
 strongest and given in the caption with its coefficient of determination (r<sup>2</sup>). The percentage differences are given between 2020 and  
 2019, 2020 and the background period, and 2020 and the predicted value from the trend. 95% confidence intervals for each estimate  
 660 are given in parentheses.



**Figure 6.** Dependence of trends (red) and difference between 2020 observations and predicted value (magenta) on detrending start year over central east China for a) AIRS CO, b) OMI PBL SO<sub>2</sub>, c) OMI tropospheric NO<sub>2</sub> and d) MODIS AOD. The solid line shows the mean of the estimate for each year and the shading shows the 95% confidence interval.



665

Figure 7. Same as Figure 5 but for southern China.

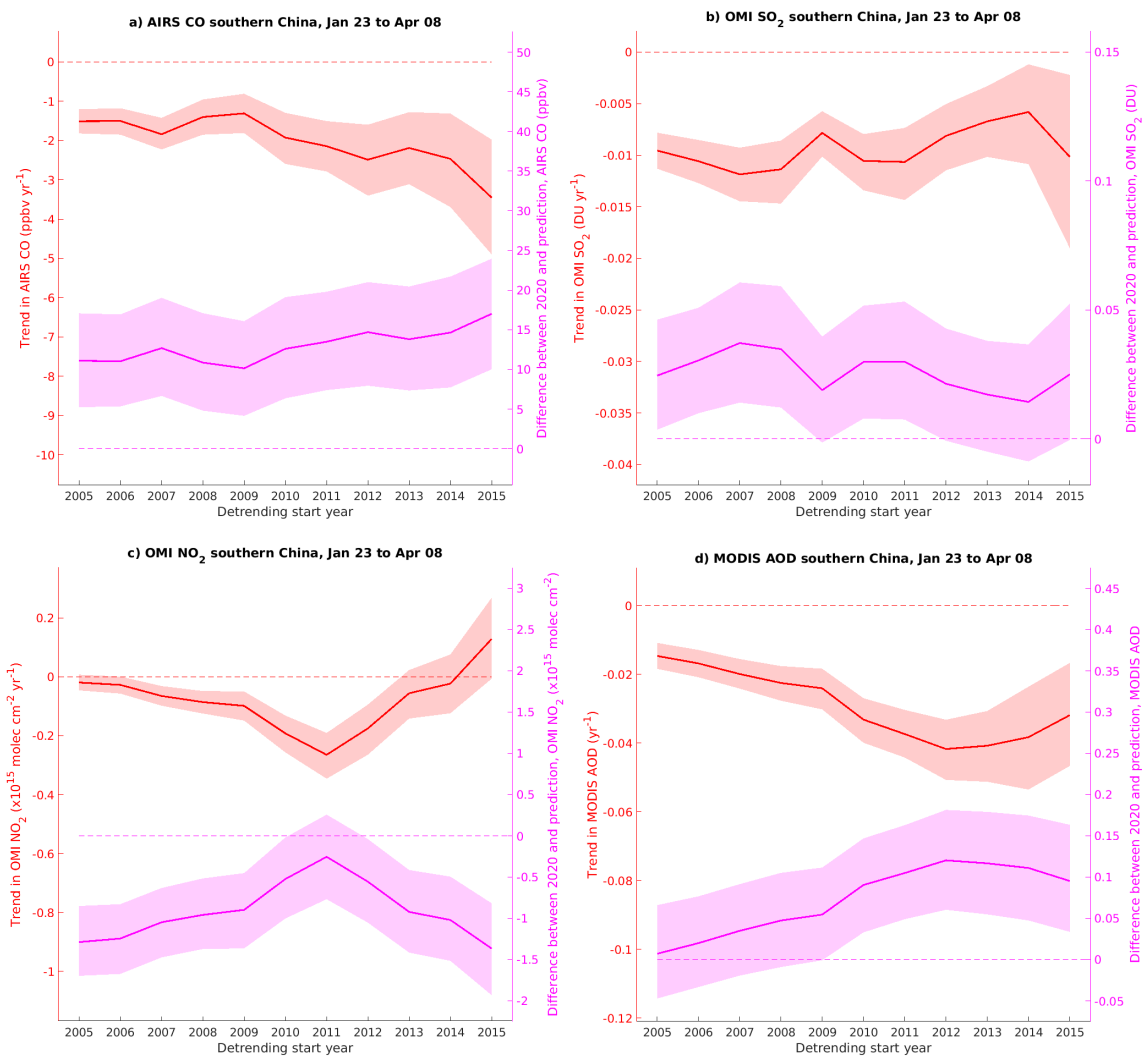


Figure 8. Same as Figure 6, but for southern China.